

# The Entropic Barrier around the Conical Intersection Seam

Johannes C. B. Dietschreit,<sup>1, a)</sup> Sebastian Mai,<sup>1, b)</sup> and Leticia González<sup>1</sup>

*Institute of Theoretical Chemistry, Faculty of Chemistry, University of Vienna, Währinger Straße 17, 1090 Vienna, Austria*

(Dated: 3 February 2026)

Conical intersections (CIs) are seen as the main mediators of nonadiabatic transitions; yet, mixed quantum-classical (MQC) simulations rarely, if ever, sample geometries with exactly degenerate electronic energies. Here we show that this behavior arises from a fundamental statistical-mechanical constraint. Using a linear vibronic coupling model, we derive the free energy along the adiabatic energy gap and demonstrate analytically that as the gap approaches zero, an infinite free-energy barrier arises around the CI seam. Molecular dynamics simulations of the methaniminium cation on the  $S_1$  surface confirm this prediction: trajectories can approach regions with small adiabatic gaps, but never reach the CI seam, even if the CI corresponds to a region of lowest potential energy. These results clarify why MQC methods successfully capture nonadiabatic behavior without sampling exact degeneracies and agree with recent findings that classical trajectories can sense the presence of CIs without visiting them.

Keywords: conical intersection, mixed quantum-classical simulation, entropic barrier

## I. INTRODUCTION

Nonadiabatic transitions mediated by conical intersections (CIs) between adiabatic electronic surfaces represent a cornerstone of modern photochemistry and photophysics. Since the seminal work by Yarkony on “diabolical” intersections,<sup>1</sup> and subsequent comprehensive reviews,<sup>2–4</sup> it has been recognized that CIs form *seams* of degeneracy in nuclear configuration space, rather than isolated points, and that nuclear motion in their vicinity cannot be described reliably within the Born–Oppenheimer approximation. In a qualitative picture of excited-state dynamics, one often invokes a molecular wave packet transiting through a CI region, thereby enabling ultrafast internal conversion.

However, a full quantum mechanical description is cumbersome and limits simulations to very small systems. A solution offer mixed quantum-classical (MQC) methods, such as trajectory surface hopping, which treat nuclei classically and model the distribution of the nuclear wave packet through ensembles of trajectories. Curiously, despite lacking a full nuclear wave function, and thus not explicitly encoding the geometric phase or the exact degeneracy manifold, MQC approaches frequently reproduce ultrafast nonadiabatic population transfer near CIs with reasonable accuracy (see, e.g., Gherib, Ryabinkin, and Izmaylov<sup>5</sup> or Malhado, Bearpark, and Hynes<sup>4</sup>). This strongly suggests that, in practice, what matters is not the nuclear coordinates reaching the exact degenerate geometry, but their passage through a region of strong nonadiabatic coupling around the CI seam. Published distributions

of the energy gap for those time steps where trajectories changed adiabatic surfaces in MQC simulations document that many hops occur far away from the CI seam; however, due to limited resolution, these histograms cannot exclude transitions occurring arbitrarily close to zero gap.<sup>6–10</sup> Even quantum-jump simulations based on Lindblad trajectories do not yield transitions at the exact degeneracy.<sup>11</sup> It could even be shown that the CI does not have to be reached, but as long as the wave packet passes through regions with sufficiently strong coupling transfer between electronic states occurs.<sup>12</sup>

A more quantitative perspective emerges from the statistical-mechanical analysis of Malhado and Hynes,<sup>13</sup> who used the Landau–Zener formula<sup>14,15</sup> to derive a closed-form expression for nonadiabatic transition probabilities for a distribution of trajectories passing near a generic CI. They showed that the transition probability depends sensitively on the direction of approach and on the local CI topography in the branching plane.<sup>3,4</sup> Furthermore, they demonstrated that trajectories undergoing state transitions pass near, but never exactly through, the CI.

In this work, we build on these insights and present a free-energy analysis showing that when nuclei are treated classically (as in most MQC schemes) and a collective variable (CV) is defined as the adiabatic energy gap, the equilibrium free energy at exactly zero gap is infinite. Thus, even though nonadiabatic transitions are enabled in the neighborhood of a CI, visiting the CI itself is statistically forbidden. We derive this result analytically for a generic linear vibronic-coupling model of a CI and discuss its implications for MQC simulations of electronically excited-state dynamics. To complement the analytical treatment, we also perform explicit molecular dynamics simulations for the methanimine cation ( $\text{CH}_2\text{NH}_2^+$ , Fig. 1a) in its first excited singlet state. For this system, it is well established that the  $S_1/S_0$  conical intersection corresponds to a point of lowest potential energy on the  $S_1$  potential energy surface (PES). To

<sup>a)</sup>Electronic mail: johannes.dietschreit@univie.ac.at; These authors contributed equally

<sup>b)</sup>Electronic mail: sebastian.mai@univie.ac.at; These authors contributed equally

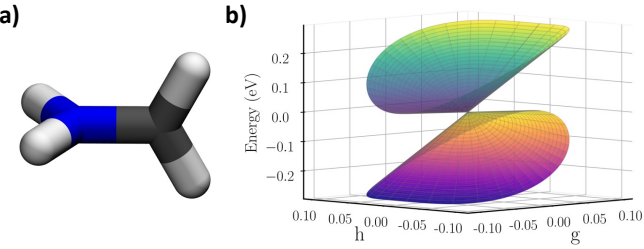


FIG. 1. Conical intersection between the ground and first excited singlet states of the methaniminium cation ( $\text{CH}_2\text{NH}_2^+$ ). (a) Optimized geometry of the minimum-energy conical intersection (MECI) corresponding to the  $\text{S}_1/\text{S}_0$  degeneracy point. (b) Three dimensional rendering of the adiabatic potential-energy surfaces in the vicinity of the MECI, shown as cut along the branching-plane coordinates  $g$  and  $h$  (gradient-difference and nonadiabatic-coupling directions) to illustrate the characteristic double-cone topography of the CI.

illustrate this, Fig. 1 shows the minimum-energy conical intersection (MECI) of  $\text{CH}_2\text{NH}_2^+$  and a visualization of the  $\text{S}_1$  and  $\text{S}_0$  potential-energy surfaces along the branching-plane coordinates. Nevertheless, despite the apparent energetic driving force toward the MECI, and thus parts of the seam, our molecular dynamics simulations demonstrate that trajectories approach the seam but never reach the exact degeneracy, fully consistent with the statistical-mechanical argument developed below.

## II. THEORY

### A. Initial Definitions

Following the derivation of Dietschreit *et al.*<sup>16</sup>, the free energy profile along a CV  $\xi(\mathbf{R})$  is defined as

$$F(z) = -k_B T \ln [\rho(z) \langle \lambda_\xi \rangle_z], \quad (1)$$

where  $\mathbf{R} = (R_1, R_2, \dots, R_{3N_a})^\top$  denotes a point in the nuclear configuration space of a system containing  $N_a$  atoms.  $\rho(z)$  is the marginal probability density of configurations satisfying  $\xi(\mathbf{R}) = z$ ,

$$\begin{aligned} \rho(z) &= \frac{\int d\mathbf{R} e^{-E(\mathbf{R})/k_B T} \delta(\xi(\mathbf{R}) - z)}{\int d\mathbf{R} e^{-E(\mathbf{R})/k_B T}} \\ &= \langle \delta(\xi(\mathbf{R}) - z) \rangle, \end{aligned} \quad (2)$$

and  $\lambda_\xi = \sqrt{\hbar^2/(2\pi k_B T m_\xi)}$  is the thermal de Broglie wavelength of the CV, with  $m_\xi$  the generalized mass in curvilinear coordinates. The notation  $\langle \cdot \rangle_z$  denotes an ensemble average at fixed  $\xi(\mathbf{R}) = z$ .

In this work, the CV is chosen as the energy gap between two consecutive adiabatic electronic states,

$$\xi(\mathbf{R}) = \Delta E_{IJ}(\mathbf{R}) = E_J(\mathbf{R}) - E_I(\mathbf{R}). \quad (3)$$

The generalized CV mass in curvilinear coordinates is

$$m_\xi^{-1} = \sum_{a=1}^{N_a} \sum_{i=1}^3 \frac{1}{M_a} \left( \frac{\partial \xi}{\partial R_{ai}} \right)^2, \quad (4)$$

where  $M_a$  is the mass of nucleus  $a$ . For the specific choice  $\xi = E_J - E_I$  this becomes

$$m_\xi^{-1}(\mathbf{R}) = \sum_{a=1}^{N_a} \sum_{i=1}^3 \frac{1}{M_a} [\mathbf{F}_I - \mathbf{F}_J]_{ai}^2, \quad (5)$$

where  $\mathbf{F}_\alpha$  denotes the nuclear forces on state  $\alpha$ . If neither adiabatic potential diverges, the associated forces remain finite, implying that  $m_\xi$  also stays finite. Because we focus on the behavior of the free energy near the CI and  $\lambda_\xi$  remains finite, it suffices to analyze the limit of  $\rho(z)$  as  $z \rightarrow 0$ .

### B. Approximating the Potential Energy Surface Near a Conical Intersection

CIs are not isolated points but multidimensional hypersurfaces (seams) where two adiabatic states become degenerate, *i.e.*,  $\Delta E_{IJ} = 0$ . The degeneracy is lifted along two linearly independent directions in nuclear coordinate space, the gradient-difference and nonadiabatic-coupling directions, which span the branching plane.<sup>1,17,18</sup> These are defined as

$$\mathbf{g}_{IJ} = \frac{\partial}{\partial \mathbf{R}} (E_J - E_I), \quad (6)$$

and

$$\mathbf{h}_{IJ} = (E_J - E_I) \left\langle \Psi_I^{\text{el}} \left| \frac{\partial}{\partial \mathbf{R}} \right| \Psi_J^{\text{el}} \right\rangle, \quad (7)$$

where  $\Psi_\alpha^{\text{el}}$  are the adiabatic electronic wavefunctions.

Near a CI, the adiabatic potential energy matrix may be represented by a linear vibronic coupling model truncated after first-order terms,<sup>19</sup>

$$\mathbf{V}(\mathbf{R}) = E_{\text{spec}}(\mathbf{q}) + \begin{pmatrix} Ag & Ch \\ Ch & Bg \end{pmatrix}, \quad (8)$$

where  $g$  and  $h$  are projections of  $\mathbf{R}$  onto the branching vectors,  $\mathbf{q}$  denotes the remaining  $3N_a - 8$  spectator modes, and  $A$ ,  $B$ , and  $C$  determine the local CI topography, namely its slope and tilt. Diagonalization gives the adiabatic energies

$$\begin{aligned} E_{J/I}(g, h, \mathbf{q}) &= E_{J/I}^{\text{CI}}(g, h) + E_{\text{spec}}(\mathbf{q}) \\ &= \frac{A + B}{2} g \pm \sqrt{\frac{(A - B)^2}{2} g^2 + C^2 h^2 + E_{\text{spec}}(\mathbf{q})}. \end{aligned} \quad (9)$$

### C. Free Energy Near the Conical Intersection

Using Eq. (9), the marginal Boltzmann distribution (the projection onto the energy gap) becomes

$$\begin{aligned}\rho_{J/I}(z) &= \frac{\iiint dg dh d\mathbf{q} e^{-E_{J/I}(g,h,\mathbf{q})/k_B T} \delta(\Delta E - z)}{\iiint dg dh d\mathbf{q} e^{-E_{J/I}(g,h,\mathbf{q})/k_B T}} \\ &= \frac{\iint dg dh e^{-E_{J/I}^{\text{CI}}(g,h)/k_B T} \delta(\Delta E - z)}{\iint dg dh e^{-E_{J/I}^{\text{CI}}(g,h)/k_B T}}. \quad (10)\end{aligned}$$

Assuming orthogonality between branching and spectator coordinates near the CI allows factorization of the  $\mathbf{q}$  integrals, which cancel in numerator and denominator.

Recognizing that the square root term in Eq. (9) equals  $\Delta E/2$ , we introduce the coordinate transformation

$$\Delta E = 2\sqrt{\frac{(A-B)^2}{2}} g^2 + C^2 h^2, \quad (11)$$

$$\phi = \text{atan2}\left(Ch, \frac{A-B}{\sqrt{2}}g\right), \quad (12)$$

which carries Jacobian

$$\mathbf{J} = \begin{pmatrix} \frac{\partial g}{\partial \Delta E} & \frac{\partial g}{\partial \phi} \\ \frac{\partial h}{\partial \Delta E} & \frac{\partial h}{\partial \phi} \end{pmatrix} = \begin{pmatrix} \frac{\cos \phi}{\sqrt{2}(A-B)} & -\frac{\Delta E \sin \phi}{\sqrt{2}(A-B)} \\ \frac{\sin \phi}{2C} & \frac{\Delta E \cos \phi}{2C} \end{pmatrix} \quad (13)$$

and

$$|\mathbf{J}| = \frac{\Delta E}{2\sqrt{2}(A-B)C}. \quad (14)$$

In these coordinates,

$$E_{J/I}(\Delta E, \phi) = \frac{1}{2\sqrt{2}} \frac{A+B}{A-B} \Delta E \cos \phi \pm \frac{\Delta E}{2}. \quad (15)$$

Substituting this into Eq. (10) yields

$$\begin{aligned}\rho_{J/I}(z) &\propto \int_0^{2\pi} d\phi \int_0^\infty d\Delta E |\mathbf{J}| e^{-E(\Delta E, \phi)/k_B T} \delta(\Delta E - z) \\ &\propto \int_0^{2\pi} d\phi \frac{z}{2\sqrt{2}(A-B)C} \\ &\times \exp\left[-\frac{1}{k_B T} \left(\frac{1}{2\sqrt{2}} \frac{A+B}{A-B} z \cos \phi \pm \frac{z}{2}\right)\right]. \quad (16)\end{aligned}$$

The angular integral is a modified Bessel function of the first kind,  $I_0(\Gamma)$ , with  $\Gamma(z) = \frac{1}{2\sqrt{2}} \frac{A+B}{A-B} \frac{z}{k_B T}$ , giving

$$\rho_{J/I}(z) \propto \frac{\pi}{\sqrt{2}(A-B)C} \times e^{\mp z/(2k_B T)} \times I_0(\Gamma(z)) \times z. \quad (17)$$

Both the exponential and  $I_0(\Gamma)$  approach unity as  $z = \Delta E \rightarrow 0$ , so that

$$\lim_{\Delta E \rightarrow 0} \rho_{J/I}(\Delta E) = 0, \quad (18)$$

agreeing with the previous finding that the CI seam is a zero measure manifold<sup>13</sup>. Since  $\langle \lambda_\xi \rangle_z$  remains finite

as  $\Delta E \rightarrow 0$ , the free energy for either electronic state diverges at the CI,

$$\begin{aligned}\lim_{\Delta E \rightarrow 0} F_{J/I}(\Delta E) &= \lim_{\Delta E \rightarrow 0} \left[ -k_B T \ln(\Delta E) \mp \frac{\Delta E}{2} \right. \\ &\quad - \frac{(A+B)^2}{32(A-B)^2} \frac{(\Delta E)^2}{(k_B T)^2} \\ &\quad \left. + O((\Delta E)^4) + \text{const.} \right] \\ &= \infty, \quad (19)\end{aligned}$$

for any nonzero temperature  $T$ , where the first line is a Taylor expansion of the free energy around zero. Thus, independent of the actual topography of the CI and even if it lies at the minimum of an adiabatic PES, the free-energy creates an insurmountable barrier, preventing a classical trajectory from reaching the exact intersection seam.

### D. Entropic Origin

To better understand the behavior of the free energy, we inspect the internal energy  $U$  and entropy  $S$ . The internal energy profile is defined as<sup>16</sup>

$$U_{J/I}(\Delta E) = \frac{\langle E_{J/I} m_\xi^{-1/2} \rangle_{\Delta E}}{\langle m_\xi^{-1/2} \rangle_{\Delta E}}. \quad (20)$$

Because both the adiabatic energies and the CV mass remain finite for all  $(g, h)$ , the internal energy does not diverge near the CI. Consequently, the divergence of the free energy must be entirely entropic:

$$S(\Delta E) = -\frac{\partial F(\Delta E)}{\partial T} = \frac{U(\Delta E) - F(\Delta E)}{T}. \quad (21)$$

As  $\Delta E \rightarrow 0$ , the available phase-space volume in the  $(g, h)$  branching plane collapses to zero, producing an entropic penalty that diverges logarithmically. This is analogous to the particle-in-a-box, where the energy levels diverge as the accessible volume shrinks to zero.

## III. COMPUTATIONAL DETAILS

All excited-state molecular dynamics simulations were performed using SHARC 4.0<sup>20</sup> and the electronic structure calculations with OPENMOLCAS v24.06.<sup>21-23</sup> Specifically, the methaniminium cation ( $\text{CH}_2\text{NH}_2^+$ ) was propagated at the state-averaged complete active space self-consistent field (SA-CASSCF) level of theory, averaging over two singlet states with a CAS(2,2) active space consisting of the  $\pi$  and  $\pi^*$  orbitals and using the cc-pVDZ basis set.<sup>24-27</sup> This minimal active space was chosen instead of the more common CAS(6,4),<sup>28</sup> as it provides superior numerical stability for our purposes and higher excited states are not relevant for the present study.

The Cholesky decomposition<sup>29</sup> was employed throughout the CASSCF calculations, and analytical gradients and nonadiabatic coupling vectors were computed at every step.

We optimized  $\text{CH}_2\text{NH}_2^+$  in the ground state and performed a frequency calculation. The resulting harmonic oscillator was used to sample 200 phase-space points from its Wigner distribution. All 200 initial conditions were manually initialized in the first excited singlet state ( $S_1$ ).

We performed adiabatic dynamics in the  $S_1$  state using the velocity–Verlet algorithm with a time step of 0.5 fs. Each trajectory was simulated for 5000 fs. Thermal effects were modeled using a Langevin thermostat set to 1000 K with a friction coefficient of 0.01 fs<sup>-1</sup> to sample the canonical ensemble. For adiabatic dynamics, surface hopping was disabled; consequently, the details of electronic propagation, decoherence correction, and kinetic energy adjustment did not affect the dynamics. Gradients and nonadiabatic coupling vectors of both states were computed and saved at every time step for subsequent analysis.

To remove nonequilibrium effects from the vertical excitation, the first 250 fs of each trajectory were discarded. Four of the 200 trajectories terminated prematurely due to CASSCF convergence failures at very high internal energies and were excluded entirely. All remaining data points were included in the analysis presented in this work. Free-energy profiles were computed using tools from the `adaptive_sampling` package.<sup>30,31</sup>

In addition to the adiabatic energy gap, we computed the minimal root-mean-squared distance (RMSD) between each instantaneous geometry and the minimum-energy conical intersection (MECI) structure. We also evaluated scalar projections of each geometry onto the unit gradient-difference vector  $\mathbf{g}$  (Eq. (6)) and the nonadiabatic-coupling vector  $\mathbf{h}$  (Eq. (7)). Geometry alignment using the Kabsch algorithm<sup>32,33</sup> and subsequent RMSD and projection calculations were implemented in PyTorch<sup>34</sup> to enable access to the Cartesian gradient of the reaction coordinates. Because two symmetry-equivalent MECI geometries exist due to the permutation of the hydrogen atoms (corresponding to rotating either the  $\text{CH}_2$  or  $\text{NH}_2$  fragment by 180° around the C–N bond), both were considered when computing RMSD and branching-plane projections. We always selected the MECI geometry that had the smaller RMSD after alignment.

#### IV. RESULTS AND DISCUSSION

The log–log histogram of the sampled adiabatic energy gap  $\Delta E$  (Fig. 2) shows a clear linear decrease in population as the gap approaches zero. This behavior is fully consistent with the theoretical prediction of Eq. (17), which also yields a linear dependence of the marginal probability density  $\rho(\Delta E)$  for small gaps. Thus, the adiabatic molecular dynamics trajectories exhibit precisely

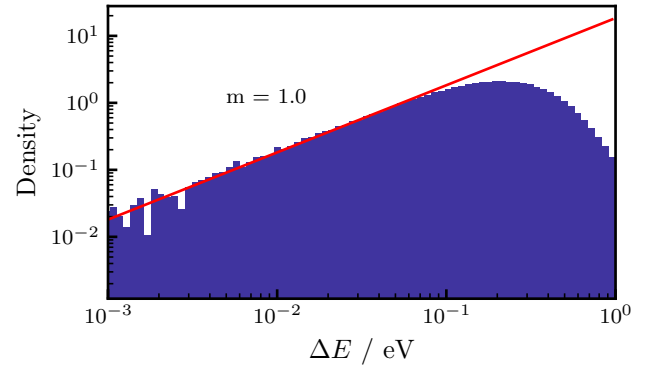


FIG. 2. Histogram of the adiabatic energy gap  $\Delta E$  between the ground and first excited singlet states from simulations of  $\text{CH}_2\text{NH}_2^+$ . In the log–log representation, the low- $\Delta E$  region exhibits a power-law behavior; the fitted slope  $m$  corresponds to the polynomial exponent governing the dependence of the density on  $\Delta E$ .

the scaling expected for a system in which the accessible configuration-space volume shrinks near a CI seam.

The free-energy analysis is shown in Fig. 3. The internal-energy profile  $U$  decreases almost perfectly linearly with the energy gap over a broad range of  $\Delta E$  values. The fluctuations at larger gaps arise from limited sampling, as trajectories rapidly leave the Franck–Condon region and move toward the  $S_1/S_0$  conical-intersection seam. As anticipated from the analytical model, the internal energy remains finite throughout: the  $S_1$  potential-energy surface is smooth in all directions except at the degeneracy itself, and the generalized CV mass is likewise finite. Consequently, there is no mechanism by which the internal energy  $U$  could diverge as  $\Delta E \rightarrow 0$ .

In contrast, the free-energy profile exhibits a more complex behavior. For most gap values, it decreases approximately linearly, mirroring the trend in  $U(\Delta E)$ . However, near  $\Delta E \approx 0.2$  eV the free energy develops a local minimum, followed by a rapid increase as the gap becomes smaller. This increase reflects precisely the divergence predicted by the linear vibronic-coupling model in Eq. (19): as the energy gap approaches zero, the entropic penalty associated with the vanishing phase-space volume dominates the free-energy expression, driving  $F(\Delta E)$  upward.

The entropic contribution is shown explicitly in the entropy profile, plotted as  $TS$  in Fig. 3. The entropy decreases monotonically with decreasing energy gap, consistent with a progressive reduction of the accessible phase-space volume in the branching-plane coordinates. Near  $\Delta E = 0$ , the decay becomes increasingly steep: the number of accessible microstates  $W$  collapses to zero, yielding

$$\lim_{\Delta E \rightarrow 0} S = \lim_{W \rightarrow 0} k_B \ln W = -\infty. \quad (22)$$

This entropic penalty associated with the vanishing

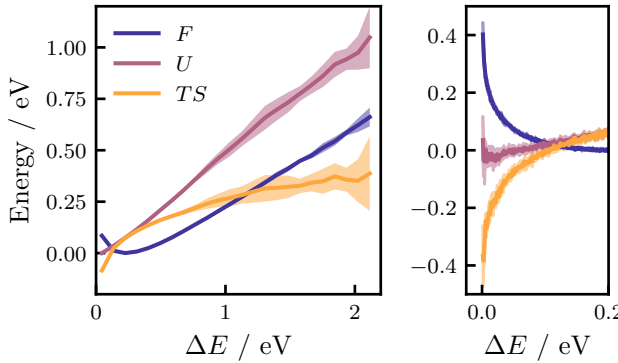


FIG. 3. Free energy  $F$ , internal energy  $U$ , and entropy  $TS$  profiles from the  $S_1$  dynamics of  $\text{CH}_2\text{NH}_2^+$  as a function of the adiabatic energy gap  $\Delta E$ . The right panel shows a magnified view of the small-gap region. The minimum of the free-energy curve as well as  $U(0)$  were shifted to zero for clarity. All energies are given in electron volts. The shaded regions indicate the standard deviation between curves obtained by splitting the 196 trajectories into batches of 28 each. The solid line represents the average of the seven curves computed this way.

configuration-space volume dominates the free-energy expression. The simulations thus confirm the central theoretical prediction: the free energy contains an entropic barrier that prevents classical nuclear trajectories from sampling configurations exactly on the CI seam.

The combined simulation and analytical results, therefore, provide a coherent picture. Although the  $S_1/S_0$  MECI in methaniminium corresponds to an energetically favorable region (*i.e.*, it corresponds to the configuration of lowest energy on the  $S_1$  surface), the free-energy barrier associated with the energy-gap CV diverges. As a consequence, the CI is never visited in practice, even in the long MQC trajectories propagated at elevated temperatures presented here. Trajectories may approach the seam arbitrarily closely, but the exact degeneracy manifold remains statistically inaccessible.

To view the same effect from a different perspective, we also computed free-energy profiles according to Eq. (1) for two additional CVs: (i) the minimal root-mean-squared deviation (RMSD) from the MECI geometry, and (ii) the difference between the instantaneous  $S_1$  energy and the  $S_1$  energy of the MECI. Both CVs quantify the distance from the MECI geometry, but do not measure the distance to higher-energy points along the CI seam. Nevertheless, the free-energy profiles shown in Fig. 4 diverge as the CV approaches zero, demonstrating that the MECI geometry itself is never visited — even though it would be the most attractive point on the  $S_1$  surface when potential energy alone is considered.

Another way to characterize the deviation from the CI is to project the Cartesian displacement vector of a configuration from the MECI onto the branching plane, which is spanned by the gradient-difference vector  $\mathbf{g}$  (Eq. (6)) and the nonadiabatic-coupling vector  $\mathbf{h}$

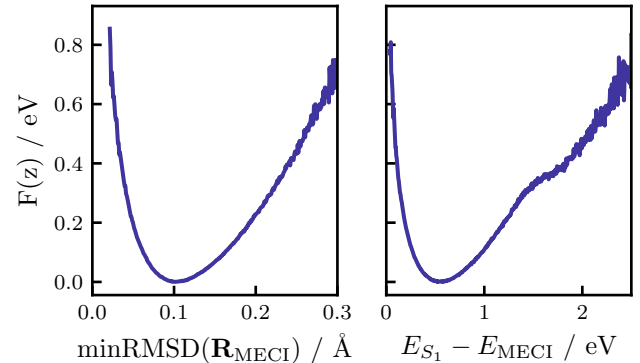


FIG. 4. Free-energy profile  $F(z)$  as a function of (left) the minimal RMSD from the MECI geometry and (right) the difference between the  $S_1$  energy and the  $S_1$  energy at the MECI.

(Eq. (7)) of the MECI geometry. The resulting scalar coordinates indicate how far a geometry lies from the MECI along each branching-plane direction; the MECI is reached only when both  $g$  and  $h$  are simultaneously zero.

The potential of mean force (PMF), defined in two dimensions as

$$A(g, h) = -k_B T \ln [\rho(g, h)] \quad (23)$$

with  $\rho(g, h)$  being the marginal Boltzmann probability density along the projected  $g$  and  $h$  values, is shown in Fig. 5. Contrary to what one might expect from the previous results, the PMF exhibits a shallow minimum displaced slightly from the origin; however, at the origin, no divergence is visible. The reason for this apparent discrepancy is the different dimensionality of this projection. In the one dimensional representations, such as  $\Delta E$ , we have effectively transformed the projection onto the  $g-h$ -plane into polar coordinates and integrated over the polar angle. The configuration space represented by the circle with a radius of zero (the CI seam) has no volume and thus carries no statistical weight. More rigorously, lower-dimensional manifolds such as the CI seam, which is a  $(3N_a - 8)$ -dimensional space, have zero measure under continuous distributions. This means that the probability for a trajectory to pass arbitrarily close by, however, is finite.

This behavior is analogous to the vanishing probability of zero relative distance in radial distribution functions or zero velocity in Maxwell–Boltzmann statistics, where geometry alone suppresses probability density even in the absence of an energetic barrier.

## V. CONCLUSION

We have presented both analytical and simulation-based evidence that, when nuclei are treated classically, there is an entropic barrier barring the simulation from

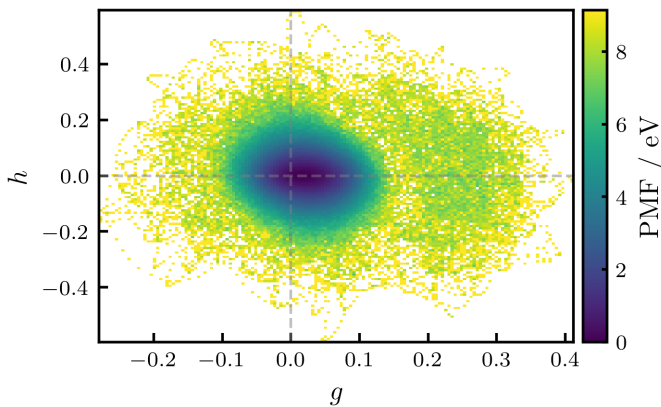


FIG. 5. Two-dimensional potential of mean force (PMF) along the projections onto the gradient-difference coordinate  $g$  and the nonadiabatic-coupling coordinate  $h$ . The dashed gray lines mark  $g = 0$  and  $h = 0$ , whose intersection corresponds to the MECI geometry.

accessing the conical-intersection (CI) seam. The gap-based free-energy framework developed here thus identifies the CI seam as effectively “forbidden territory” for classical trajectories, even though its topography usually brings trajectories into its vicinity. The linear vibronic coupling model predicts that the marginal probability density vanishes as  $\Delta E \rightarrow 0$ , and our molecular dynamics simulations of methaniminium ( $\text{CH}_2\text{NH}_2^+$ ) confirm that trajectories can approach arbitrarily small gaps but never reach the exact degeneracy.

Our findings complement the recent observations of Karmakar, Thakur, and Jain,<sup>35</sup> who concluded that purely classical trajectories can *sense* the presence of a CI without ever arriving at it. Taken together, these results reinforce the notion that although the CI seam exerts a strong influence on nonadiabatic dynamics, it remains statistically inaccessible by trajectories evolving on adiabatic surfaces with classical nuclear motion.

From the perspective of computational dynamics, our findings underscore that MQC simulations rely on sampling the vicinity of the CI, where nonadiabatic couplings are large, rather than populating the degeneracy manifold itself. This has direct implications for interpreting reaction pathways, transition-state analogies in excited states, and designing enhanced-sampling strategies for nonadiabatic processes. Future work may explore how quantum nuclear effects, such as zero-point vibrations or tunneling, could modify or partially lift the free-energy barrier discussed in this contribution.

## ACKNOWLEDGMENTS

The authors thank Carolin Müller for the code to visualize the CI.

## DATA AVAILABILITY STATEMENT

All simulation data and analysis scripts have been deposited in the Zenodo archive <https://doi.org/10.5281/zenodo.18196244>.

- <sup>1</sup>D. R. Yarkony, Rev. Mod. Phys. **68**, 985–1013 (1996).
- <sup>2</sup>W. Domcke, D. R. Yarkony, and H. Köppel, *Conical Intersections: Electronic Structure, Dynamics and Spectroscopy* (WORLD SCIENTIFIC, 2004).
- <sup>3</sup>W. Domcke and D. R. Yarkony, Annual Review of Physical Chemistry **63**, 325–352 (2012).
- <sup>4</sup>J. P. Malhado, M. J. Bearpark, and J. T. Hynes, Frontiers in Chemistry **2** (2014), 10.3389/fchem.2014.00097.
- <sup>5</sup>R. Gherib, I. G. Ryabinkin, and A. F. Izmaylov, Journal of Chemical Theory and Computation **11**, 1375–1382 (2015).
- <sup>6</sup>B. G. Levine and T. J. Martínez, Annual Review of Physical Chemistry **58**, 613–634 (2007).
- <sup>7</sup>M. Barbatti, Journal of Chemical Theory and Computation **17**, 3010–3018 (2021).
- <sup>8</sup>S. Mukherjee and M. Barbatti, Results in Chemistry **4**, 100521 (2022).
- <sup>9</sup>D. V. Cofer-Shabica, M. F. S. J. Menger, Q. Ou, Y. Shao, J. E. Subotnik, and S. Faraji, Journal of Chemical Theory and Computation **18**, 4601–4614 (2022).
- <sup>10</sup>S. Mukherjee, R. S. Mattos, J. M. Toldo, H. Lischka, and M. Barbatti, The Journal of Chemical Physics **160** (2024), 10.1063/5.0203636.
- <sup>11</sup>M. C. Anderson, A. J. Schile, and D. T. Limmer, The Journal of Chemical Physics **157** (2022), 10.1063/5.0102891.
- <sup>12</sup>C. A. Farfan and D. B. Turner, The Journal of Physical Chemistry A **123**, 7768–7776 (2019).
- <sup>13</sup>J. a. P. Malhado and J. T. Hynes, Journal of Chemical Physics **145**, 194104 (2016).
- <sup>14</sup>L. Landau, Physikalische Zeitschrift der Sowjetunion, 46 (1932).
- <sup>15</sup>C. Zener, Proceedings of the Royal Society of London. Series A, Containing Papers of a Mathematical and Physical Character **137**, 696–702 (1932).
- <sup>16</sup>J. C. B. Dietschreit, D. J. Diestler, and R. Gómez-Bombarelli, J. Chem. Theory Comput. **19**, 5369–5379 (2023).
- <sup>17</sup>D. R. Yarkony, J. Phys. Chem. A **105**, 6277–6293 (2001).
- <sup>18</sup>D. R. Yarkony, J. Chem. Phys. **123** (2005), 10.1063/1.2114827.
- <sup>19</sup>G. J. Atchity, S. S. Xantheas, and K. Ruedenberg, J. Chem. Phys. **95**, 1862–1876 (1991).
- <sup>20</sup>S. Mai, B. Bachmair, L. Gagliardi, H. G. Gallmetzer, L. Grünewald, M. R. Hennefarth, N. M. Hoyer, F. A. Korsaye, S. Mausenberger, M. Oppel, T. Piteša, S. Polonius, E. S. Gil, Y. Shu, N. K. Singer, M. X. Tiefenbacher, D. G. Truhlar, D. Vörös, L. Zhang, and L. González, “SHARC4.0: Surface hopping including arbitrary couplings — program package for non-adiabatic dynamics,” <https://sharc-md.org/> (2025).
- <sup>21</sup>I. Fdez. Galván, M. Vacher, A. Alavi, C. Angeli, F. Aquilante, J. Autschbach, J. J. Bao, S. I. Bokarev, N. A. Bogdanov, R. K. Carlson, L. F. Chibotaru, J. Creutzberg, N. Dattani, M. G. Delcey, S. S. Dong, A. Dreuw, L. Freitag, L. M. Frutos, L. Gagliardi, F. Gendron, A. Giussani, L. González, G. Grell, M. Guo, C. E. Hoyer, M. Johansson, S. Keller, S. Knecht, G. Kovačević, E. Källman, G. Li Manni, M. Lundberg, Y. Ma, S. Mai, J. P. Malhado, P. Å. Malmqvist, P. Marquetand, S. A. Mewes, J. Norell, M. Olivucci, M. Oppel, Q. M. Phung, K. Pierloot, F. Plasser, M. Reiher, A. M. Sand, I. Schapiro, P. Sharma, C. J. Stein, L. K. Sørensen, D. G. Truhlar, M. Ugandi, L. Ungur, A. Valentini, S. Vancoillie, V. Veryazov, O. Weser, T. A. Wesołowski, P.-O. Widmark, S. Wouters, A. Zech, J. P. Zobel, and R. Lindh, Journal of Chemical Theory and Computation **15**, 5925–5964 (2019).
- <sup>22</sup>F. Aquilante, J. Autschbach, A. Baiardi, S. Battaglia, V. A. Borin, L. F. Chibotaru, I. Conti, L. De Vico, M. Delcey, I. Fdez. Galván, N. Ferré, L. Freitag, M. Garavelli, X. Gong,

S. Knecht, E. D. Larsson, R. Lindh, M. Lundberg, P. Å. Malmqvist, A. Nenov, J. Norell, M. Odelius, M. Olivucci, T. B. Pedersen, L. Pedraza-González, Q. M. Phung, K. Pierloot, M. Reiher, I. Schapiro, J. Segarra-Martí, F. Segatta, L. Seijo, S. Sen, D.-C. Sergentu, C. J. Stein, L. Ungur, M. Vacher, A. Valentini, and V. Veryazov, *The Journal of Chemical Physics* **152**, 214117 (2020).

<sup>23</sup>G. Li Manni, I. Fdez. Galván, A. Alavi, F. Aleotti, F. Aquilante, J. Autschbach, D. Avagliano, A. Baiardi, J. J. Bao, S. Battaglia, L. Birnoschi, A. Blanco-González, S. I. Bokarev, R. Broer, R. Cacciari, P. B. Calio, R. K. Carlson, R. Carvalho Couto, L. Cerdán, L. F. Chibotaru, N. F. Chilton, J. R. Church, I. Conti, S. Coriani, J. Cuéllar-Zuquin, R. E. Daoud, N. Dattani, P. De-cleva, C. de Graaf, M. G. Delcey, L. De Vico, W. Dobrutz, S. S. Dong, R. Feng, N. Ferré, M. Filatov(Gulak), L. Gagliardi, M. Garavelli, L. González, Y. Guan, M. Guo, M. R. Henne-farth, M. R. Hermes, C. E. Hoyer, M. Huix-Rotllant, V. K. Jaiswal, A. Kaiser, D. S. Kaliakin, M. Khamesian, D. S. King, V. Kochetov, M. Krośnicki, A. A. Kumaar, E. D. Larsson, S. Lehtola, M.-B. Lepetit, H. Lischka, P. López Ríos, M. Lund-berg, D. Ma, S. Mai, P. Marquetand, I. C. D. Merritt, F. Mon-torsi, M. Mörchen, A. Nenov, V. H. A. Nguyen, Y. Nishimoto, M. S. Oakley, M. Olivucci, M. Oppel, D. Padula, R. Pandharkar, Q. M. Phung, F. Plasser, G. Raggi, E. Rebolini, M. Reiher, I. Ri-valta, D. Roca-Sanjuán, T. Romig, A. A. Safari, A. Sánchez-Mansilla, A. M. Sand, I. Schapiro, T. R. Scott, J. Segarra-Martí, F. Segatta, D.-C. Sergentu, P. Sharma, R. Shepard, Y. Shu, J. K. Staab, T. P. Straatsma, L. K. Sørensen, B. N. C. Tenorio, D. G. Truhlar, L. Ungur, M. Vacher, V. Veryazov, T. A. Voß, O. Weser, D. Wu, X. Yang, D. Yarkony, C. Zhou, J. P. Zobel, and R. Lindh, *Journal of Chemical Theory and Computation* **19**, 6933–6991 (2023).

<sup>24</sup>B. O. Roos, *International Journal of Quantum Chemistry* **18**, 175–189 (1980).

<sup>25</sup>H.-J. Werner and P. J. Knowles, *The Journal of Chemical Physics* **82**, 5053–5063 (1985).

<sup>26</sup>K. Andersson, P.-Å. Malmqvist, and B. O. Roos, *The Journal of Chemical Physics* **96**, 1218–1226 (1992).

<sup>27</sup>T. H. Dunning, *The Journal of Chemical Physics* **90**, 1007–1023 (1989).

<sup>28</sup>J. Westermayr, M. Gastegger, M. F. S. J. Menger, S. Mai, L. González, and P. Marquetand, *Chemical Science* **10**, 8100–8107 (2019).

<sup>29</sup>T. B. Pedersen, F. Aquilante, and R. Lindh, *Theoretical Chemistry Accounts* **124**, 1–10 (2009).

<sup>30</sup>A. Hulm, J. C. B. Dietschreit, and C. Ochsenfeld, *J. Chem. Phys.* **157** (2022), 10.1063/5.0095554.

<sup>31</sup>A. Hulm, J. C. B. Dietschreit, R. Schiller, L. Yannick, A. Stan, and L. Glinkina, “adaptive\_sampling: Adaptive sam-pling algorithms for molecular transitions,” [https://github.com/ochsenfeld-lab/adaptive\\_sampling/](https://github.com/ochsenfeld-lab/adaptive_sampling/).

<sup>32</sup>W. Kabsch, *Acta Crystallographica Section A* **32**, 922–923 (1976).

<sup>33</sup>W. Kabsch, *Acta Crystallographica Section A* **34**, 827–828 (1978).

<sup>34</sup>A. Paszke, S. Gross, F. Massa, A. Lerer, J. Bradbury, G. Chanan, T. Killeen, Z. Lin, N. Gimelshein, L. Antiga, A. Desmaison, A. Kopf, E. Yang, Z. DeVito, M. Raison, A. Tejani, S. Chilamkurthy, B. Steiner, L. Fang, J. Bai, and S. Chintala, “Py-torch: An imperative style, high-performance deep learning li-brary,” (2019), arXiv:1912.01703 [cs.LG].

<sup>35</sup>S. Karmakar, S. Thakur, and A. Jain, *The Journal of Chemical Physics* **160** (2024), 10.1063/5.0197381.

<sup>36</sup>R. Mansour, S. Mukherjee, M. Pinheiro, J. A. Noble, C. Jouvet, and M. Barbatti, *Physical Chemistry Chemical Physics* **24**, 12346–12353 (2022).